Efficient computation of time-resolved transfer functions for imaging in turbid media

Andrew Dunn* and Charles DiMarzio

Center for Electromagnetics Research, Department of Electrical and Computer Engineering, Northeastern University, Boston, Massachusetts 02115

Received December 1, 1994; revised manuscript received June 16, 1995; accepted July 24, 1995

The transfer function of a turbid medium such as biological tissue provides a method of analyzing the spatial resolution of a time-resolved tissue imaging system. A method is presented of calculating the transfer function with the use of a Monte Carlo simulation. The model allows the computation of the time-resolved line-spread function of a sample of thickness d from a simulation of thickness $d/2$ by use of reciprocity under certain conditions, and the transfer function can then be computed from the line-spread function. Results with this method agree with previously published theoretical and experimental results. © 1996 Optical Society of America

1. INTRODUCTION

Imaging of objects embedded in tissue at optical frequencies is possible because objects such as tumors have different optical properties from those of the surrounding tissue.[1] Optical imaging is limited, however, by the highly scattering nature of tissue in the visible and near-infrared region of the spectrum. As a light beam propagates through tissue, it will broaden as a result of scattering and decay as a result of absorption. The strong scattering in tissue leads to a wide range of paths traveled by the photons, and time-resolved transillumination imaging methods use the time of flight as an indication of path length to yield information about the presence of hidden objects such as tumors.[2–4] Without time-of-flight information the spatial resolution of the image will be low.

In time-resolved transillumination imaging a short-pulse laser is incident normally on the tissue, with the detector located behind the tissue, collinear with the source. The laser and the detector are scanned together in the transverse (x and y) directions, and a two-dimensional image is formed. If a tumor is present between the source and the detector, there is a different number of transmitted photons at the positions below the tumor, since it has different optical properties from those of the surrounding tissue. In a clear medium the loss of signal would be determined entirely by the absorption coefficients along a straight line through the sample. If the tumor has a higher absorption coefficient than that of the ambient tissue and thus a lower transmission $T = \exp(-\mu_a d)$, it will cast a dark shadow. In a scattering medium this technique is limited by the detection of photons scattered around the tumor.[5]

To obtain the best image, one must distinguish between those photons that are scattered around an object and those that take a direct path to the detector. Because the highly scattered photons must travel farther to go around an object, they will arrive at the detector later than the photons with more direct paths. Therefore, if a time gate is set on the detector, only the photons that have deviated least from the optical axis can be selectively detected, which improves the resolution of the image.[1,6,7]

For extremely short times there will be few photons detected, but the image resolution will be greater. For longer times the number of photons will be greater, but the resolution will be lower. Therefore the integration time will vary, depending on the required resolution.

The spatial resolution of an imaging system is commonly characterized by its modulation transfer function (MTF), which is the modulus of the Fourier transform of the point spread function (PSF). Therefore one can determine the spatial resolution by first calculating the PSF of the system.

The MTF curve at each integration time has a slightly different shape, with its amplitude determined by the number of transmitted photons. Traditionally each MTF curve is normalized to its value at zero frequency, but in this paper the MTF will not be normalized since its amplitude will represent the strength of the signal at the detector. For any given spatial frequency the optimum time gate will be that time for which the MTF is largest. The peak amplitude for all spatial frequencies will define an envelope that represents the resolution limit for the tissue. Associated with each setting of the time gate is a particular PSF and therefore a MTF. For short time gates the PSF and the MTF have low amplitudes because fewer photons are detected. The PSF is narrow, and therefore the MTF is wide. For larger time gates more photons will be detected, which increases the amplitudes of the PSF and the MTF, but the PSF will be wider and the MTF will be narrower. The Fourier transform of the best image is obtained by the application of an appropriate deconvolution to the data with the highest MTF at each point in the transform.

2. POINT-SPREAD-FUNCTION COMPUTATION: PRODUCT-OF-PROBABILITIES METHOD

The PSF of an optical system is a measure of the degree to which light is spread out. An image can be formed

0740-3232/96/010065-06$06.00 © 1996 Optical Society of America

through a convolution of the PSF with the transmission function of the system. In the case of transillumination imaging the PSF is a measure of the photon distribution on the central plane $z = d/2$. For highly scattering tissue the photons will be more widely distributed. The PSF is proportional to the probability of a photon traveling from its initial position at the origin (0, 0, 0), to any point $(x, y, d/2)$ on the central plane $z = d/2$, multiplied by the probability of travel from the central plane, $(x, y, d/2)$, to the detector located at point $(0, 0, d)$. The two-dimensional distribution of probabilities for all points $(x, y, d/2)$ is the PSF. Computation of the PSF in this way requires that the probabilities for both the upper half $(0 \le z \le d/2)$ and the lower half $(d/2 \le z \le d)$ be calculated.

Monte Carlo simulations for realistic tissue thicknesses require a large number of photon paths to be traced for accurate data, which results in large computation times. If the probability for the lower half of the tissue is rewritten in terms of an equivalent probability expressed in terms of the upper half, the PSF can be computed from the results of a simulation of half of the desired thickness. Because the ratio of the number of photons into the number of photons out is exponential in thickness, the time saving is significant.

To show that this is a valid approach, let the six-element vector $\mathbf{q} = (x, y, z, \mu_x, \mu_y, \mu_z)$ represent the position (x, y, z) and the direction of propagation (μ_x, μ_y, μ_z) of a photon, where μ_x, μ_y, and μ_z are the directional cosines of the photon. If $\mathbf{q}_0 = (x_0, y_0, z_0, \mu_{x0}, \mu_{y0}, \mu_{z0})$ is another point and direction, then $P(\mathbf{q} \mid \mathbf{q}_0)$ is the probability of travel from $\mathbf{q}_0$ to $\mathbf{q}$. Four vectors $\mathbf{q}_0$, $\mathbf{q}_{1A}$, $\mathbf{q}_{1B}$, $\mathbf{q}_2$ are defined as

$$\begin{aligned} \mathbf{q}_0 &= (0, 0, 0, 0, 0, 1), \\ \mathbf{q}_{1A} &= (x, y, d/2, \mu_x, \mu_y, \mu_z), \\ \mathbf{q}_{1B} &= (x, y, d/2, -\mu_x, -\mu_y, \mu_z), \\ \mathbf{q}_2 &= (0, 0, d, 0, 0, 1). \end{aligned} \tag{1}$$

These four vectors are represented graphically in Fig. 1, where the tissue has been split into two halves along the central plane. The total probability of traveling from the origin to the detector at $(0, 0, d)$ through any point $(x, y, d/2)$ on the central plane is

$$P(\mathbf{q}_2 \mid \mathbf{q}_0) = \int P(\mathbf{q}_{1A} \mid \mathbf{q}_0) P(\mathbf{q}_2 \mid \mathbf{q}_{1A}) \mathrm{d}\mathbf{q}_{1A}. \tag{2}$$

This represents the probability of traveling from the origin to any point on the plane $z = d/2$ in any direction and then to the detector at $(0, 0, d)$, integrated over all intermediate points. In order to find $P(\mathbf{q}_2 \mid \mathbf{q}_0)$ with a sample of thickness $d/2$, we must determine information about the second half, $P(\mathbf{q}_{1A} \mid \mathbf{q}_2)$, from the data of the first half. If the direction of propagation of a photon in the second half is reversed under the assumption that the photon starts at $(0, 0, d)$, the signs of the directional cosines μ_x and μ_y must be reversed and

$$P(\mathbf{q}_2 \mid \mathbf{q}_{1A}) = P(\mathbf{q}_{1B} \mid \mathbf{q}_2). \tag{3}$$

In Fig. 1 the vector $\mathbf{q}_{1B}$ is shown on both the upper and lower halves of the tissue, which demonstrates that if we flip the lower half to match the upper half, the probability for the second half can be written in terms of a probability in the top half as

$$P(\mathbf{q}_{1B} \mid \mathbf{q}_2) = P(\mathbf{q}_{1B} \mid \mathbf{q}_0) \tag{4}$$

and Eq. (2) can be written in terms of probabilities from the upper half,

$$P(\mathbf{q}_2 \mid \mathbf{q}_0) = \int P(\mathbf{q}_{1A} \mid \mathbf{q}_0) P(\mathbf{q}_{1B} \mid \mathbf{q}_0) \mathrm{d}\mathbf{q}, \tag{5}$$

where $\mathrm{d}\mathbf{q}$ represents the integral over x, y, μ_x, and μ_y.

Equation (5) gives the probability for all photon paths from the source to the detector through all points $(x, y, d/2)$ in all directions (μ_x, μ_y, μ_z). To find the two-dimensional PSF, we integrate over μ_x and μ_y:

$$P(\mathbf{q}_2 \mid \mathbf{q}_0) = \int_{-1}^{1} \int_{-1}^{1} P(\mathbf{q}_{1A} \mid \mathbf{q}_0) P(\mathbf{q}_{1B} \mid \mathbf{q}_0) \mathrm{d}\mu_x \mathrm{d}\mu_y. \tag{6}$$

This will give the two-dimensional time-independent PSF. We find the time-resolved PSF by incorporating the time of flight for each photon into the probability such that $P(\mathbf{q}_b, t_2 \mid \mathbf{q}_a, t_1)$ represents the probability of starting at position and direction $\mathbf{q}_a$ at time t_1 and being a position and direction $\mathbf{q}_b$ at time t_2, assuming that $t_2 > t_1$. The time-resolved PSF is all combinations of t_1 and t_2 such that

$$t_2 + t_1 \le \tau, \tag{7}$$

where τ is the total allowed travel time through the full sample of thickness d. Equation (6) becomes

$$\begin{aligned} P(\mathbf{q}_2, \tau \mid \mathbf{q}_0, 0) = \int_{-1}^{1} \int_{-1}^{1} \int_{0}^{\tau} \int_{0}^{\tau - t_1} & P(\mathbf{q}_{1A}, t_1 \mid \mathbf{q}_0, 0) \\ & \times P(\mathbf{q}_{1B}, t_2 \mid \mathbf{q}_0, 0) \mathrm{d}t_2 \mathrm{d}t_1 \mathrm{d}\mu_x \mathrm{d}\mu_y. \end{aligned} \tag{8}$$

3. MONTE CARLO SIMULATION

The PSF was computed from the results of a Monte Carlo simulation. The basis for the Monte Carlo simulation

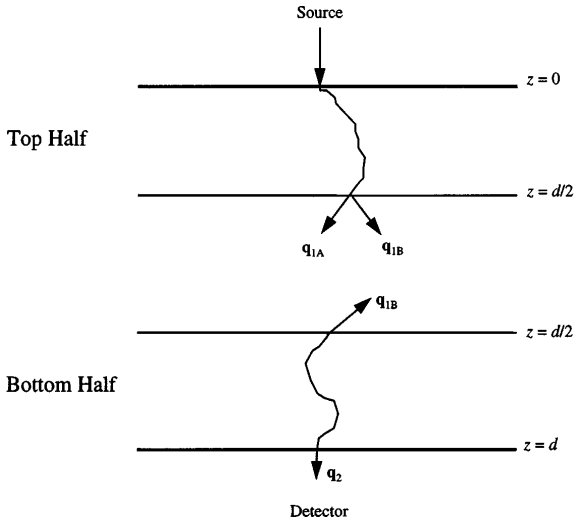

Fig. 1. Geometry for the product-of-probabilities method. The vectors $\mathbf{q}_{1A}$, $\mathbf{q}_{1B}$, and $\mathbf{q}_2$ each represent a point and a direction of a photon. The tissue is split along the plane $z = d/2$.

was the program written by Wang and Jacques, MCML (Monte Carlo Multi-Layer Tissue).[8] The code was modified as part of the present work to compute the time of flight for each photon packet and record the transmission as a function of radius, exit angle, and time. In each simulation individual photons are traced through the time until they are either transmitted or reflected out of the tissue or are completely absorbed. As each photon reaches the lower surface, $z = d/2$, the transmission is recorded in a three-dimensional array in cylindrical coordinates, $T(r, \beta, t)$, where r refers to the radial distance from the optical axis, β refers to the modified direction of travel, and t refers to the time. The simulation was performed on a sample of thickness $d/2$, so that when a photon is referred to as exiting the tissue, it is meant that the photon is exiting the top half of the tissue sample. Cylindrical symmetry is assumed for the PSF, so a photon exiting at $(x, y, d/2)$ is counted in a bin defined by $r = \sqrt{x^2 + y^2}$. Assuming cylindrical symmetry requires that

$$P(\mathbf{q}_{1A} \,|\, \mathbf{q}_0) = P(\mathbf{q}'_{1A} \,|\, \mathbf{q}_0)\,, \tag{9}$$

provided that $\mathbf{q}'_{1A} = R_\theta(\mathbf{q}_{1A})$, where R_θ is the rotation operator,

$$R_\theta = \begin{bmatrix} \cos\theta & \sin\theta & 0 & 0 & 0 & 0 \\ -\sin\theta & \cos\theta & 0 & 0 & 0 & 0 \\ 0 & 0 & 1 & 0 & 0 & 0 \\ 0 & 0 & 0 & \cos\theta & \sin\theta & 0 \\ 0 & 0 & 0 & -\sin\theta & \cos\theta & 0 \\ 0 & 0 & 0 & 0 & 0 & 1 \end{bmatrix}. \tag{10}$$

In order to define the angle of each photon exiting the tissue as a meaningful one-dimensional parameter, we define $\mathbf{r}_{xy}$ as the location of the photon on the x–y plane at the bottom surface of the tissue ($z = d/2$) and $\mathbf{s}$ as the direction of photon propagation just prior to exiting the tissue. $\mathbf{r}_{xy}$ and $\mathbf{s}$ are defined as

$$\mathbf{r}_{xy} = x\hat{x} + y\hat{y}\,, \qquad \mathbf{s} = \mu_x\hat{x} + \mu_y\hat{y} + \mu_z\hat{z}\,. \tag{11}$$

The exit angle is characterized by the cosine of the angle between r_{xy} and s, β:

$$\beta = \frac{\mathbf{r}_{xy}\cdot\mathbf{s}}{|\mathbf{r}_{xy}\cdot\mathbf{s}|} = \left(\frac{x\hat{x} + y\hat{y}}{\sqrt{x^2 + y^2}}\right)\cdot(\mu_x\hat{x} + \mu_y\hat{y} + \mu_z\hat{z}) = \frac{x\mu_x + y\mu_y}{\sqrt{x^2 + y^2}}\,. \tag{12}$$

The range of β is -1 to 1, and this is represented graphically in Fig. 2. The bottom view [Fig. 2(a)] shows the different values of β for a photon exiting at $\mathbf{r}_{xy}$ on the x–y plane at $z = d/2$. β is equal to zero when $\mathbf{r}_{xy}$ and $\mathbf{s}$ are perpendicular, and $\beta = 1$ when they are in the same direction. The three-dimensional view in Fig. 2(b) illustrates how $\mathbf{s}$ defines a sphere and the sphere is then divided into strips determining the values of β.

To compute the time-resolved line-spread function (LSF), we convert Eq. (8) to a summation. We combine the integration over x and y into a single summation by matching the transmission probabilities of the two halves according to the angle parameter. The angles are paired as follows:

$$\begin{gathered} \beta = -1 \leftrightarrow \beta = +1\,, \\ \beta = -1 + \Delta\beta \leftrightarrow \beta = +1 - \Delta\beta\,, \\ \vdots \leftrightarrow \vdots \\ \beta = 0 \leftrightarrow \beta = 0\,, \\ \vdots \leftrightarrow \vdots \\ \beta = +1 - \Delta\beta \leftrightarrow \beta = -1 + \Delta\beta\,, \\ \beta = +1 \leftrightarrow \beta = -1\,. \end{gathered} \tag{13}$$

In terms of the indices on β, this pairing means matching each β_i with $N_\beta - \beta_i$, where N_β is the total number of divisions of β. The sum then becomes

$$P(\mathbf{q}_2, \tau \,|\, \mathbf{q}_0, 0) = \sum_{\beta_i=1}^{N_\beta}\sum_{t_n=1}^{N_t}\sum_{t_m=1}^{N_t - t_n} T(r_i, \beta_i, t_n)T(r_i, N_\beta - \beta_i, t_m)\,, \tag{14}$$

where N_t is the total allowed time gate and $T(r, \beta, t)$ represents the transmission at location r, direction β, and time t. This summation yields the time-resolved LSF on the plane $z = d/2$ for photons entering at the origin (0, 0, 0) and exiting directly below the entrance point (0, 0, d). The summation in Eq. (14) was computed in a separate program that was written to compute the time-resolved LSF at different times from the output of the Monte Carlo simulation.

Equation (14) provides a method of computing the PSF for a sample of thickness d with the use of results from a simulation of thickness $d/2$. It accounts for all photon paths through the tissue except for those that cross

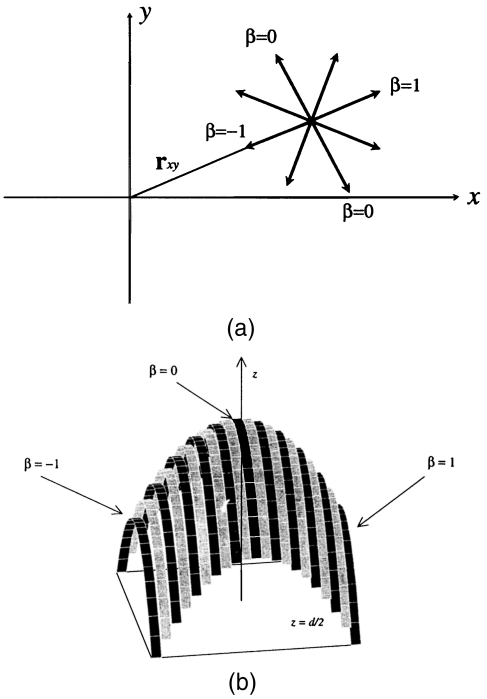

Fig. 2. Graphical representation of the characterization of the photon exit direction. (a) Bottom view. The arrows represent different directions $\mathbf{s}$, and the corresponding values for β are indicated for a particular $\mathbf{r}_{xy}$. (b) Three-dimensional view. The values for β are distributed into strips ranging from -1 to 1.

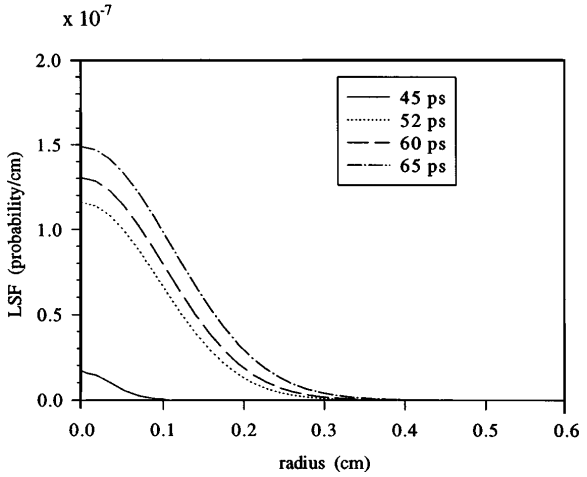

Fig. 3. Time-resolved LSF for a thickness of 1 cm. The optical properties used in the simulation are $\sigma_s = 100\ \text{cm}^{-1}$, $\sigma_a = 0.5\ \text{cm}^{-1}$, and $g = 0.97$.

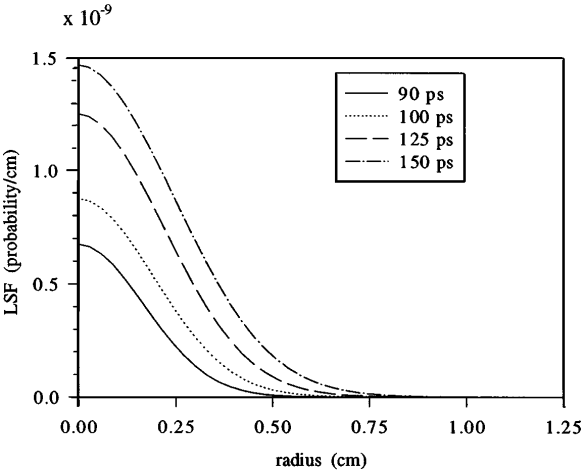

Fig. 4. Time-resolved LSF for a thickness of 2 cm. The optical properties are the same as those in Fig. 3.

the midplane of the tissue $z = d/2$ multiple times. This limits the applicability of this method to those geometries in which the number of photons crossing the midplane more than once is small compared with the total number of detected photons.

4. RESULTS

To illustrate the approach, we ran the Monte Carlo simulation and computed LSF and MTF curves for different time gates. Figure 3 shows the LSF at different times for a sample 1 cm thick. The absorption coefficient σ_a, the scattering coefficient σ_s, and the anisotropy g were chosen to be representative of human breast tissue,[9–11] and the interface between the bottom surface of the tissue and the exiting medium was assumed to be index matched to prevent any Fresnel reflections, since the two halves of the tissue are split only for the purpose of the simulation. To obtain the plot in Fig. 3, we ran the Monte Carlo simulation on a sample 0.5 cm thick, and the LSF for the 1-cm sample was calculated with the product-of-probabilities method. The plot shows that as the time gate is increased, the amplitude of the LSF increases, but it also spreads out since the photons have traveled longer paths to the detector. This is demonstrated by the full width at half-maximum values (FWHM), which are 0.1, 0.2, 0.24, and 0.26 cm for the time gates.

Figure 4 contains plots of the LSF for a sample 2 cm thick with the same optical properties as those of the sample in Fig. 3. The LSF is more spread out than it was for the thinner sample and has an amplitude 2 orders of magnitude lower, on account of the increased thickness. In addition, the time gate necessary for the first photons to arrive is considerably longer in the thicker sample.

Since the sample in Fig. 3 is thin, a few photons arrive at the detector at $t = 45$ ps, close to the unscattered photon flight time. The amplitude of the LSF at this

Table 1. Percentages of Photons Crossing the Midplane More Than Once[a]

Depth d (cm)	$N > 1$	$N = 1$
1	5.66%	94.34%
2	13.0%	87.0%
4	45.1%	54.9%

[a] N indicates the number of times each photon crosses the plane $z = d/2$.

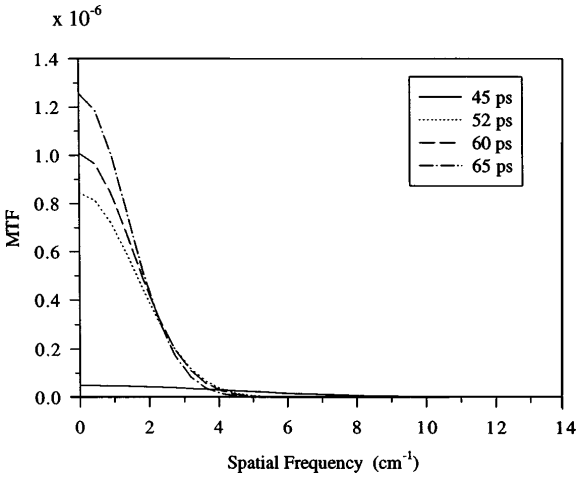

Fig. 5. Time-resolved MTF for the 1-cm case.

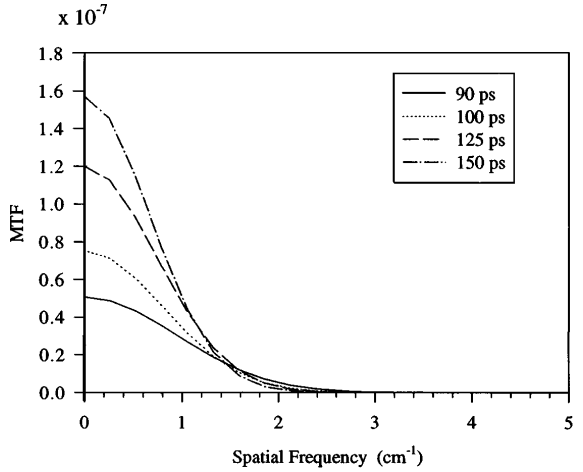

Fig. 6. Time-resolved MTF for the 2-cm case.

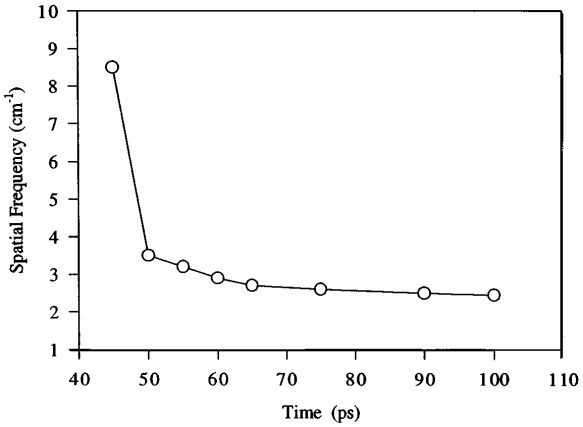

Fig. 7. Spatial frequency versus detector time gate for the 1-cm case.

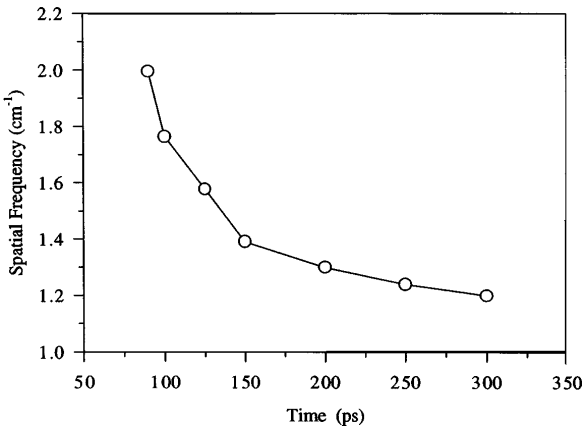

Fig. 8. Spatial frequency versus detector time gate for the 2-cm case.

time is a factor of 10 lower than that of the longer times and is considerably narrower.

For each of the above cases the Monte Carlo simulation was run on samples of thickness $d/2$. This method excludes those photons that would cross the central plane $z = d/2$ multiple times. To verify the validity of the model and the limitations that the exclusion of these photons imposes, we used the Monte Carlo simulation to determine the percentage of photons that cross the central plane more than once in traveling through a sample of thickness d. As photons propagated through the tissue, the number of times that each photon crossed the midplane was counted. For those photons reaching the bottom surface and exiting the tissue in a circle of radius less than 1 mm, the percentage crossing the midplane multiple times was calculated.

Table 1 shows the percentage of photons crossing once and the percentage crossing more than once for several thicknesses. The optical properties used were the same as those of the other simulations ($\sigma_s = 100$ cm^{-1}, $\sigma_a = 0.5$ cm^{-1}, $g = 0.97$). As the thickness increases, the fraction of detected photons having crossed the midplane more than once increases. Therefore the method of splitting the tissue along the central plane is valid, provided that the fraction crossing only once is large compared with the fraction crossing multiple times.

With the tissue geometries used in the calculation of the LSF 94% and 87% of all the photons were accounted for. At a depth of 4 cm, however, the percentage of photons with multiple crossings is 45%. This suggests an upper limit of approximately 200 optical depths for this model, where 1 optical depth is the reciprocal of the attenuation coefficient, $1/(\sigma_s + \sigma_a)$.

The MTF curves for each sample were calculated from the LSF data. The plots in Figs. 5 and 6 show that as the integration time decreases, the amplitude of the MTF decreases but also decays more gradually. For any given spatial frequency we determine the optimal time gate by selecting the time gate with the largest amplitude at that spatial frequency. For example, if the desired spatial resolution is less than 2 cm^{-1} for the 1-cm sample (Fig. 5), the optimum time gate would be 65 ps. However, if greater resolution is required, a shorter time would yield the resolution and would provide the strongest signal. The MTF of the thin 1-cm sample demonstrates that a shorter integration time yields a broader MTF, and as the unscattered photon time is approached, the MTF will be flat.

To assess the spatial resolution as a function of integration time, we calculated the spatial frequency at which the MTF curve has a value of 0.1 of its maximum. The results, shown in Figs. 7 and 8, indicate that the spatial resolution increases sharply with a decreasing time gate. As expected, the resolution is greatest for the 1-cm sample. The plots indicate that subcentimeter resolution is possible for samples 2 cm thick and submillimeter resolution is attainable for 1-cm samples, in agreement with previous results.[12,13] Achievement of this resolution, however, depends on extremely short detection times and is possible only when the fraction of detected photons is above the noise threshold.

Previous results based on Monte Carlo simulations performed by DeHaller and Depeursinge[14] have indicated a minimum resolution of 3 mm for a 2-cm-thick sample of breast tissue. The resolution obtained with the current method agrees with this result, as demonstrated in Fig. 8, where the spatial resolution, based on the MTF, is approximately 2 cm^{-1} or, based on the FWHM of the PSF, is approximately 3.8 mm. The Monte Carlo results in Ref. 14 were verified with experimental data, indicating resolutions ranging from 3 to 10 mm, depending on the time gate, for a 2-cm-thick sample.[15]

Chen[4] determined resolutions comparable with the current results for 1-cm-thick samples. The 1–2-mm resolutions are close to those indicated in Fig. 7 obtained with the product-of-probabilities method.

5. CONCLUSIONS

A technique for calculating the spatial resolution of a time-resolved imaging system has been presented with the use of Monte Carlo simulations. When the sample is less than 200 optical depths in thickness, one can compute the tissue transfer function with a Monte Carlo simulation of a sample of half the desired thickness, provided that the position, the time, and the exit angle of the transmitted photons are known, by matching the two halves. The final result is then all combinations of photons whose travel times add up to less than the detector time gate.

*Present address, Biomedical Engineering Program, University of Texas at Austin, Austin, Texas 78712.

REFERENCES

1. J. Hebden and R. Kruger, "Transillumination imaging performance: spatial resolution simulation studies," Med. Phys. **17,** 41–47 (1990).
2. L. Wang, X. Liang, P. Ho, and R. Alfano, "Time and Fourier-space gated optical imaging and thick turbid media," in *Photon Migration and Imaging in Random Media and Tissues*, R. R. Alfano and B. Chance, eds., Proc. Soc. Photo-Opt. Instrum. Eng. **1888,** 2–5 (1993).
3. K. Yoo, B. Das, and R. Alfano, "Imaging of a translucent object hidden in a highly scattering medium from the early portion of the diffuse component of a transmitted laser pulse," Opt. Lett. **17,** 958–960 (1992).
4. Y. Chen, "Characterization of the image resolution for the first-arriving-light method," Appl. Opt. **33,** 2544–2552 (1994).
5. J. Hebden, "A time-of-flight breast imaging system: spatial resolution performance," in *Time-Resolved Spectroscopy and Imaging of Tissues*, B. Chance and A. Katzer, eds., Proc. Soc. Photo-Opt. Instrum. Eng. **1431,** 225–231 (1991).
6. K. Carson, Y. Wickramasinghe, and P. Rolfe, "Experimental study of the spatial resolution for time resolved near infrared imaging," in *Quantification and Localization Using Diffuse Photons in a Highly Scattering Medium*, B. Chance, ed., Proc. Soc. Photo-Opt. Instrum. Eng. **2082,** 10–19 (1993).
7. A. Gandjbakhche, R. Nossal, and R. Bonner, "Theoretical study of resolution limits for time resolved imaging of human breast," in *Advances in Laser and Light Spectroscopy to Diagnose Cancer and Other Diseases*, R. R. Alfano, ed., Proc. Soc. Photo-Opt. Instrum. Eng. **2135,** 176–185 (1994).
8. L. Wang and S. Jacques, *Monte Carlo Modeling of Light Transport in Multi-layered Tissues in Standard C,* (M. D. Andersen Cancer Center, University of Texas, Houston, Tex., 1992).
9. W. Cheong, S. Prahl, and A. Welch, "A review of the optical properties of biological tissues," IEEE J. Quantum Electron. **26,** 2166–2185 (1990).
10. V. Peters, D. Wyman, M. Patterson, and G. Frank, "Optical properties of normal and diseased human breast tissues in the visible and near infrared," Phys. Med. Biol. **35,** 1317–1334 (1990).
11. H. Key, E. Davies, P. Jackson, and P. Wells, "Optical attenuation characteristics of breast tissues at visible and near-infrared wavelengths," Phys. Med. Biol. **36,** 579–590 (1991).
12. J. Hebden, "Evaluating the spatial resolution performance of a time-resolved optical imaging system," Med. Phys. **19,** 1081–1087 (1992).
13. F. Liu, K. Yoo, and R. Alfano, "Ultrafast laser-pulse transmission and imaging through biological tissue," Appl. Opt. **32,** 554–558 (1993).
14. E. DeHaller and C. Depeursinge, "Time resolved breast transillumination: Monte Carlo simulation and comparison with experimental results," in *Photon Migration and Imaging in Random Media and Tissues*, R. R. Alfano and B. Chance, eds., Proc Soc. Photo-Opt. Instrum. Eng. **1888,** 191–200 (1993).
15. E. DeHaller and C. Depeursinge, "Time-resolved breast transillumination: comparison of theoretical and experimental image resolution," in *Quantification and Localization Using Diffuse Photons in a Highly Scattering Medium*, B. Chance, ed., Proc. Soc. Photo-Opt. Instrum. Eng. **2082,** 2–9 (1993).